RSC Advances

PAPER

View Article Online
View Journal | View Issue

Cite this: *RSC Adv.*, 2024, **14**, 27174

One-pot synthesis of tetrahydropyrimidinecarboxamides enabling *in vitro* anticancer activity: a combinative study with clinically relevant brain-penetrant drugs†

Dipti B. Upadhyay,‡[a] Joaquina Nogales,‡[b] Jaydeep A. Mokariya,[a] Ruturajsinh M. Vala,[a] Vasudha Tandon,[b] Sourav Banerjee *[b] and Hitendra M. Patel *[a]

Received 7th June 2024
Accepted 14th August 2024

DOI: 10.1039/d4ra04171b

rsc.li/rsc-advances

In this study, we describe a one-pot three-component synthesis of bioactive tetrahydopyrimidinecarboxamide derivatives employing lanthanum triflate as a catalyst. Out of the synthesized compounds, **4f** had the most potent anti-cancer activity and impeded cell cycle progression effectively. Anti-cancer bioactivity was observed in **4f** against liver, breast, and lung cancers as well as primary patient-derived glioblastoma cell lines. Compound **4f** effectively inhibited the 3D neurosphere formation in primary patient-derived glioma stem cells. Specifically, **4f** exhibited synergistic cytotoxicity with the EGFR inhibitor that is the clinical epidermal growth factor receptor inhibitor osimertinib. **4f** does not exhibit anti-kinase activity and is cytostatic in nature, and further work is needed to understand the true molecular target of **4f** and its derivatives. Through our current work, we establish a promising tetrahydopyrimidinecarboxamide-based lead compound with anti-cancer activity, which may exhibit potent anti-cancer activity in combination with specific clinically relevant small molecule kinase inhibitors.

1 Introduction

Dihydropyrimidinones (DHPMs) produced *via* the Biginelli reaction have received significant attention owing to their diverse biological applications, such as acetylcholinesterase inhibitors,[1] HIV-1 replication inhibitors,[2] urease inhibitors,[3] calcium channel blockers,[4] antimicrobial agents,[5] antioxidant agents,[6] nonsteroidal RORα agonists,[7] anti-cancer cytotoxic agents,[8] and antitubercular agents.[9] From this DHPM family of compounds, monastrol emerged as a key lead compound.[10,11] Monastrol has significant anticancer properties (Fig. 1) and prevents metastasis by impeding the movement of kinesin spindle protein Eg5,[12] which associates with microtubules of the mitotic spindle[13] and engages in intracellular transport and cell division.[14] Dihydropyrimidine derivatives allosterically inhibit Eg5-mediated microtubule organisation and drive the anti-metastatic activities.[15] Monastrol was first observed to cause cell cycle disruption in Xenopus models[16] and later monastrol and its derivatives were reported to have robust anti-proliferative activities against cancer cells.[17] Multiple research groups have since developed several DHPMs that exhibited antiproliferative properties against other human solid tumour cell lines (Fig. 1).

In the current study, we wanted to utilise our long-standing successful strategy[11,18–25] of utilising the Biginelli reaction to synthesize benzyloxy derivatives of DHPM to obtain new bioactive, anti-cancer compounds. The benzyloxyphenyl group has diverse medicinal properties, including antimicrobial,[26] antitubercular,[27] antifungal,[28] and anticancer activities.[11,29–32] Similarly, the incorporation of a 1,2,3-triazole moiety into various compounds has shown significant pharmacological potential, such as anticancer,[33–38] antimicrobial,[33,39] anti-inflammatory,[40] antitubercular,[41] anti-HIV,[42] and antiviral effects.[33] Studies have shown that 1,2,3-triazoles can exert anticancer effects through various mechanisms, such as enzyme inhibition and targeting receptor tyrosine kinases.[43–48]

The aim of this study was to utilise the Biginelli reaction to integrate the 1,4-disubstituted 1,2,3-triazole and benzyloxyphenyl group using a wide variety of catalysts like Lewis acids, salts, or ionic liquids to generate phenyloxymethyl-1,2,3-triazole derivatives with potentially distinct anticancer attributes. Furthermore, we employed lanthanum triflate as a catalyst that acts as a Lewis acid resulting in excellent yield over a short reaction period. From the series of compounds synthesized, we identified one derivative to have

[a]*Department of Chemistry, Sardar Patel University, Vallabh Vidyanagar, Gujarat, India. E-mail: hm_patel@spuvvn.edu*

[b]*Division of Cancer Research, School of Medicine, University of Dundee, Dundee DD1 9SY, UK. E-mail: s.y.banerjee@dundee.ac.uk*

† Electronic supplementary information (ESI) available. See DOI: https://doi.org/10.1039/d4ra04171b

‡ These authors contributed equally.

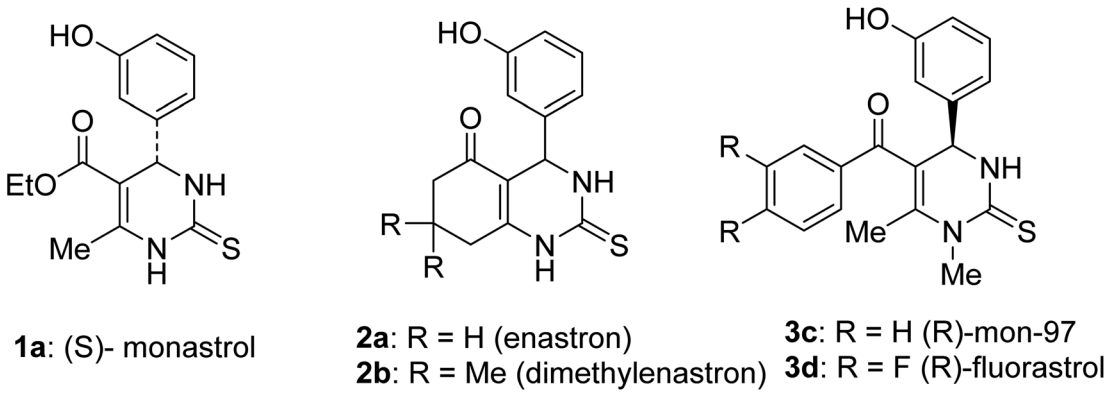

Fig. 1 Bioactive dihydropyrimidinones (DHPMs).

potent anti-proliferative effects across multiple solid tumour cell lines and effectively impede the cell cycle with a reduction in cancer stem cell numbers in primary patient-derived cancer cells. The derivative also induced cytotoxicity in combination with FDA-approved clinical drugs thus suggesting a novel paradigm in our efforts to utilise the Biginelli reaction and green catalysts to generate anti-cancer compounds.

2 Results and discussion

2.1 Chemistry

The synthesis of benzyl triazolyl methoxy derivative of DHPM was carried out by the multicomponent reaction of the 4-((1-benzyl-1*H*-1,2,3-triazole-4-yl)methoxy)benzaldehyde, different acetoacetanilide derivatives, and urea/thiourea. The inclusion

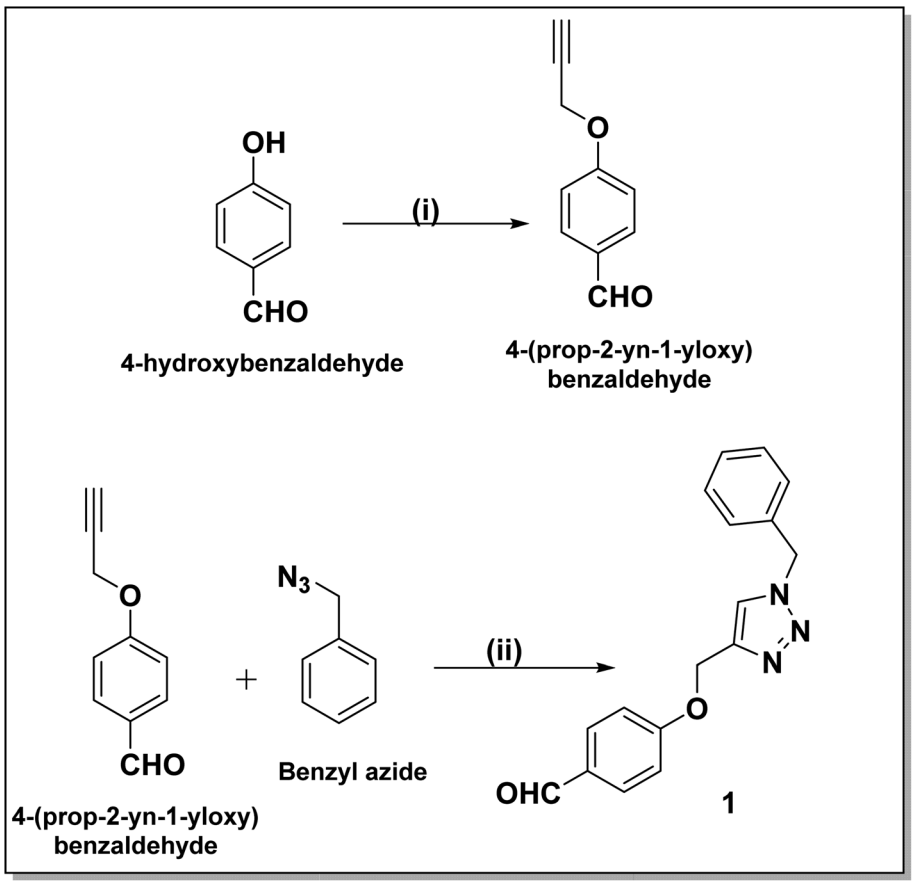

Scheme 1 Synthesis of the 4-[(1-benzyl-1*H*-1,2,3-triazol-4-yl)methoxy]benzaldehyde (a) reaction conditions: (i) propargyl bromide, acetone, K_2CO_3, 2 h. (ii) $CuSO_4$, sodium ascorbate, DMF/water (8 : 2), 3 h.

of this aldehyde in the reaction is anticipated to enhance its biological applications. Compound **1** which is 4-((1-benzyl-1*H*-1,2,3-triazole-4-yl)methoxy)benzaldehyde, was prepared through a click reaction involving 4-(prop-2-yn-1-yloxy)benzaldehyde and benzyl azide, as illustrated in Scheme 1. The reaction was carried out by employing 10 mol% lanthanum triflate as a catalyst and under a heating environment at 100 °C for about 1–1.5 h, which resulted in good-to-excellent yields.

Our initial study was carried out both in solvent-free conditions as well as under various solvents like ethanol, acetonitrile, ethylene dichloride, tetrahydrofuran, dimethylformamide, and water (Table 1). The effect of solvent amount and required time was investigated. Among the mentioned solvents, ethanol gave the best outcomes with an excellent yield. It was found that using more solvent caused the reaction to take 3.5 hours to complete under reflux conditions. However, when the minimum amount of ethanol (0.5 ml) was utilized at 100 °C, the reaction mixture solidified within the 35 min but remained slightly incomplete. Hence, we decided to use 0.5 ml more ethanol to the reaction mixture and stir for 25 minutes. This successfully completed the reaction, and we observed a high-yield conversion of DHPM. Having set optimized parameters, $La(OTf)_3$-catalyzed 20 derivatives of dihydopyrimidones were synthesized by employing various substrates (Table 2). All the synthesized compounds were characterized by ^1H nuclear magnetic resonance (NMR), $13C\{^1H\}$[35] attached proton test,[49] and either high-resolution mass spectra (HRMS) or liquid chromatography-mass spectrometry (LCMS) analysis (see ESI†).

After improving the reaction, the substrate scope for the $La(OTf)_3$-catalyzed synthesis of dihydropymidine derivatives was investigated by changing the different acetoacetanilide derivatives. Substitution of the acetoacetanilides gave a slight variation in the time of reaction and yield of the product (Table 2). Compound **4a** was obtained with an excellent 97% yield in one hour (Table 2, entry 1), while when 3,4-$(CF_3)_2$ substituted acetoacetanilide derivative was employed under the same reaction condition, a slightly decreased yield of 79% was observed (Table 2, entry 11) in 1.5 h. When chloro substituted acetoacetanilide derivatives were used as a substrate, a comparatively good yield was observed than the methyl-substituted acetoacetanilide derivatives (Table 2). In the case of trifluoro methyl substituted acetoacetanilide derivative, it takes 1.5 h to complete the reaction. Based on the above-discussed facts, it was observed that substitutions on the acetoacetanilide have shown great influence on the reaction time as well as in isolated yield (Scheme 2).

Table 1 Effect of solvent on the reaction[a]

Entry	Solvent	Temp.	Time	Conversion relative to aldehyde[b]
1	CH_3CN[c]	Reflux	4 h	100%
2	DCE[c]	Reflux	4 h	Incomplete
3	THF[c]	Reflux	4 h	Incomplete
4	DMF[c]	Reflux	3 h	Mixture of product
5	Water[c]	Reflux	5 h	Incomplete
6	Ethanol[c]	Reflux	3.5 h	100%
7	Ethanol[d]	100 °C	1 h	100%
8	Solvent-free	100 °C	30 min	Incomplete
9	Catalyst-free	100 °C	30 min	Mixture of product

[a] Abbreviations: DCE, 1,2-dichloroethane; DMF, dimethylformamide; TLC, thin-layer chromatography; THF, tetrahydrofuran. Reaction condition: 1 mmol 4-((1-benzyl-1*H*-1,2,3-triazole-4-yl)methoxy) benzaldehyde **1c**, 1.1 mmol acetoacetanilide derivative **2c**, 1.2 mmol urea 3, and 0.1 mmol $La(OTf)_3$. [b] Observation from TLC analysis. [c] More than 0.5 ml solvent. [d] 0.5 ml solvent.

Table 2 Synthesis of benzyloxy DHPMs by the multicomponent reaction of 1 mmol 4-((1-benzyl-1*H*-1,2,3-triazole-4-yl)methoxy) benzaldehyde **1**, 1.1 mmol of acetoacetenilide derivatives **2(a–k)**, 1.2 mmol urea derivative (**3(a–b)**; X = O/S), and 0.1 mmol $La(OTf)_3$

Entry	–R	X	Product	Time (h)	Yield[a] (%)
1	–H	O	**4a**	1	97
2	2-Cl	O	**4b**	1	89
3	3-Cl	O	**4c**	1	90
4	4-Cl	O	**4d**	1	91
5	4-F	O	**4e**	1.5	88
6	3-CF_3	O	**4f**	1.5	91
7	2-CH_3	O	**4g**	1	87
8	4-CH_3	O	**4h**	1	86
9	2-OCH_3	O	**4i**	1	91
10	4-OCH_3	O	**4j**	1	89
11	3,4-$(CF_3)_2$	O	**4k**	1.5	79
12	–H	S	**4l**	1	94
13	2-Cl	S	**4m**	1	92
14	3-Cl	S	**4n**	1	89
15	4-Cl	S	**4o**	1	95
16	4-F	S	**4p**	1.5	85
17	3-CF_3	S	**4q**	1.5	86
18	2-CH_3	S	**4r**	1	88
19	4-CH_3	S	**4s**	1	90
20	2-OCH_3	S	**4t**	1	88

[a] Isolated yield.

The Biginelli reaction is an example of an acid-catalysed three-component reaction. In the first step of the mechanism, the acid protonates the aldehyde. The nucleophilic NH_2 group from urea then attacks the electrophilic aldehyde, leading to the formation of an *N*-acyliminium ion intermediate with the release of a water molecule. Next, the enol form of the β-keto amide attacks the *N*-acyliminium ion, resulting in the formation of a ureide intermediate. This intermediate subsequently converts into the final product (Scheme 3).

2.2 Biological evaluation

2.2.1 Establishing a potential relationship between structure and biological activity of dihydropymidine derivatives. To determine the biological relevance of these molecules *in vitro*, a cell viability assay was conducted on all synthesised compounds in triplicates at 25 μM against human cell line U87 MG. Out of the 20 molecules tested, **4f** had the maximum potency (Fig. 2A). MDA-MB-231, A549, and HEPG2 cell lines, as well as primary patient derived glioblastoma cells GBM6 and GBM22, were used to assess the anti-cancer properties of **4f** *in vitro* using cell viability assays. After 72 h incubation, cell viability was measured, and the EC_{50} values for **4f** in MDA-MB-

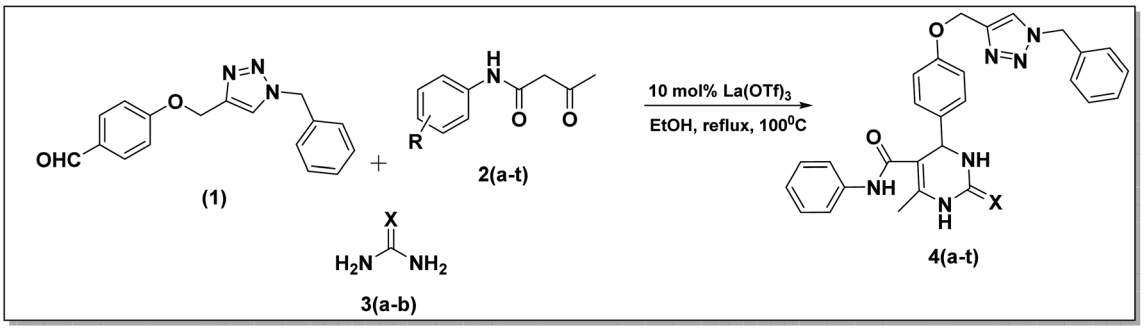

Scheme 2 Multicomponent synthesis of dihydropyrimidinones from 4-((1-benzyl-1*H*-1,2,3-triazole-4-yl)methoxy)benzaldehyde **1**, acetoacetenilide derivatives **2(a–t)**, and urea derivative **3(a–b)**.

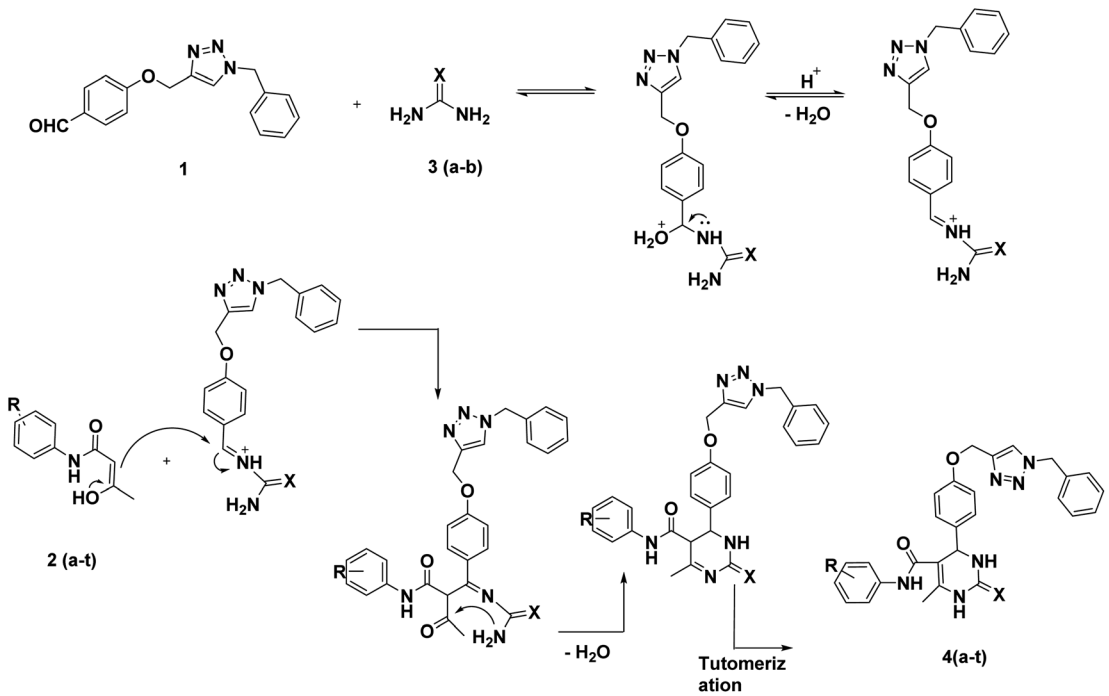

Scheme 3 Plausible mechanism of $La(OTf)_3$ catalyzed synthesis of DHPMs.

231 is 10.43 μM, A549 is 38.07 μM, HepG2 is 10.5 μM, GBM22 is 31.23 μM, and GBM6 is 22.82 μM (Fig. 2B). Since **4f** treatment leads to reduced cell numbers over 48–96 hours, we wanted to query whether **4f** function is cytotoxic or cytostatic. Hence, we carried out an assay to observe induction of apoptosis. We treated GBM6 cells with 25 μM of **4f** and utilised FDA-approved drug crenolanib as a positive control. 10 μM of crenolanib induced significant apoptosis in GBM6 cells, however, **4f** did not induce apoptotic cell death suggesting that **4f** may be cytostatic in nature (ESI Fig. S1†).

2.2.2 4f causes significant cell cycle delay in cancer cells. Since **4f** did not induce apoptosis in cancer cells, we enquired if the cytostatic function observed of **4f** could be due to the induction of cell cycle defects. For this purpose, we utilised asynchronous GBM6 cells and treated then with or without 15 or 25 μM **4f** over 16 hours. The cells were harvested post-treatment, fixed with ice-cold 70% ethanol, and the DNA content were labelled with propidium iodide. Following this, cell cycle stages of the cells were analysed using flow cytometry. Interestingly, **4f** treatment led to a dose-dependent increase in G1 and G2/M population of cells with a significant decrease in S-phase cells (Fig. 3). This clearly suggests that the cytostatic function of **4f** is indeed driven by induction of cell cycle delays in cancer cells.

2.2.3 Combination with clinically relevant brain-penetrant drugs. Since **4f** induces cytostatic effects through cell cycle impediment, we wanted to test if a combination with clinical drugs could promote synergism in inducing cancer cell death. For this purpose, we tested **4f** in two different cell lines (U87 MG and GBM6) in combination with PI-103, buparlisib,

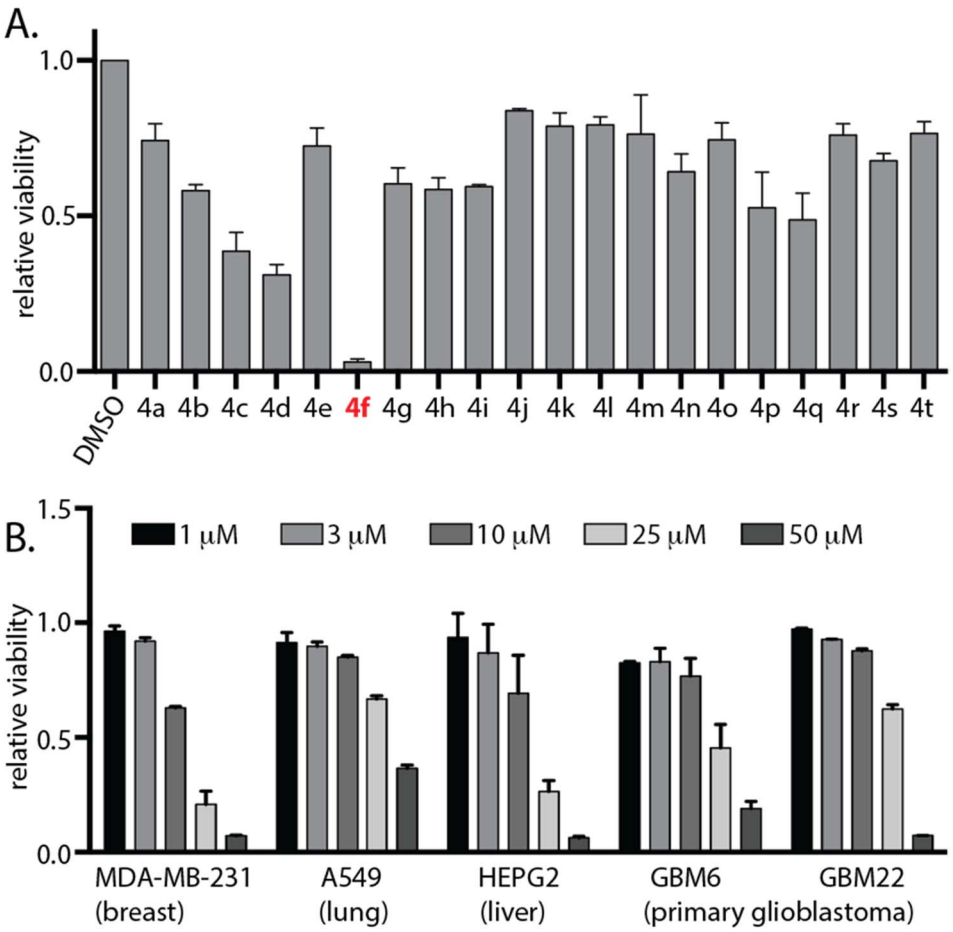

Fig. 2 **4f** exhibits anti-cancer activity in diverse cancer cell lines. (A) Cell viability of a panel of DHPM derivatives **4a–t** at 25 μM against human U87 cell line was assessed after 96 hours using the CellTiter 96 AQueous Non-Radioactive Cell Proliferation Assay kit. Viability of DMSO-treated cells was used as a control. Data are represented as fold viability of DMSO-treated control. (B) Indicated cell lines were treated with various doses of **4f** for 72 hours and their viability was measured using CellTiter 96 AQueous Non-Radioactive Cell Proliferation Assay kit. Viability of DMSO-treated cells was used as control. Data are represented as fold viability of DMSO-treated control for each cell line with $n = 3$ biological replicates. See also ESI Fig. S1.†

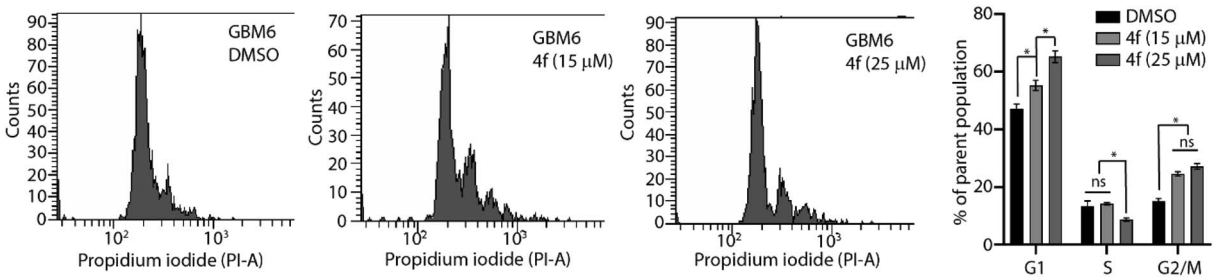

Fig. 3 **4f** exhibits cell cycle defects in GBM6 cells. Asynchronous GBM6 cells were treated with various doses of **4f** for 16 hours and the cell cycle distribution was analysed using propidium iodide and quantified using flow cytometry. * Indicates statistical significance compared to DMSO-treated control cell population; one-way ANOVA with Tukey's multiple comparison; ns: not significant.

abemaciclib, bozitinib, marizomib, nilotinib, and osimertinib (Fig. 4A–G). Interestingly, **4f** induced potent cytotoxicity in combination with nilotinib, and osimertinib (Fig. 4F and G) in the cells. While an additive combination effect was observed across all drugs with **4f**, the synergistic effect seen in combination with EGFR inhibitor osimertinib was very robust and observed across both cell types.

2.2.4 Establishing cytotoxicity in glioblastoma stem 3D neurospheres. To further determine whether **4f** treatment could impact a 3D glioma stem cell culture system, we treated

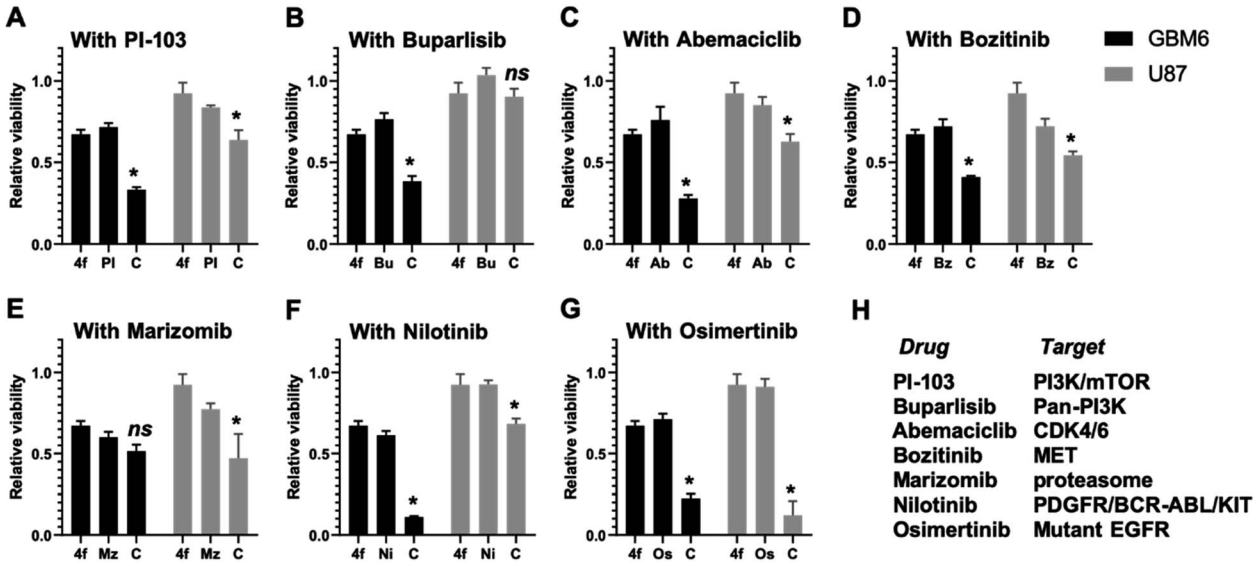

Fig. 4 **4f** induces enhanced cytotoxicity in combination with specific clinically relevant brain-penetrant small molecule inhibitors. U87 and GBM6 cells were treated with **4f** alone (10 and 25 μM respectively) or clinically relevant brain-penetrant drugs alone (A) PI-103 100 nM, (B) buparlisib 500 nM, (C) abemaciclib 1 μM, (D) bozitinib 7 μM, (E) marizomib 400 nM, (F) nilotinib 5 μM, (G) osimertinib 2 μM, or a combination C of both for 48 hours and cell viability was analysed by CellTiter 96 AQueous Non-Radioactive Cell Proliferation Assay kit. Viability of DMSO-treated cells was used as control. Data are represented as fold viability of DMSO-treated control for each cell line (* indicates statistical significance compared to each single compound treatment; one-way ANOVA with Dunnett's multiple comparison; ns: not significant). Same dataset for **4f** was used across all combination studies from (A)–(G). (H) Table lists the cellular targets of the respective clinically relevant brain-penetrant drugs.

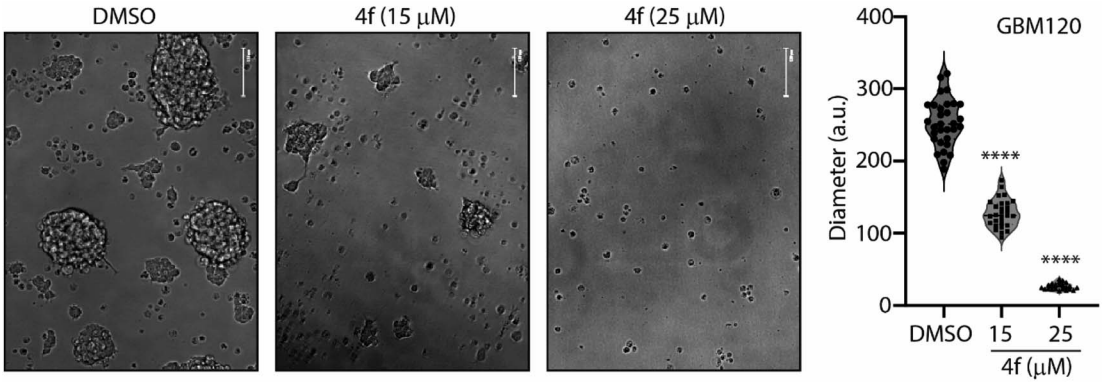

Fig. 5 Compound **4f** induces anti-glioma activity in 3D glioblastoma cell cultures. GBM120 cancer stem cells were treated with either DMSO or 15 μM or 25 μM or **4f** for 13 days and neurospheres were allowed to form. A representative image of neurospheres is shown. Scale bar = 125 μm. The diameter of the neurospheres were quantified using ImageJ. The significance of the differences was measured using one-way ANOVA with Tukey's multiple comparisons for $n = 3$ biological replicates; ****$p < 0.0001$.

GBM120 glioma stem cell lines with 15 and 25 μM **4f** for 13 days. **4f** treated GBM120 neurospheres were significantly smaller in size compared to DMSO control as observed under bright field (Fig. 5), and neurosphere formation was drastically reduced at the highest concentration (Fig. 5).

2.2.5 ***In silico*** **ADMET prediction.** The most crucial stage in the process of discovering and developing new drugs involves anticipating the ADME (Absorption, Distribution, Metabolism, and Excretion) properties. *In silico* ADMET prediction of most bioactive compound **4f** has been performed and their drug-likeness has been assessed through ADME prediction. The most potent compound and their prediction of drug-likeness are mentioned in Table 3. The physicochemical property value of **4f** lies in the zone of various filters (Table 3). The molecule **4f** shows good drug likeness properties as it follows Lipinski, veber, egan and muegge rule. There are two violations in terms of molecular weight and molar refractivity observed in the Ghose rule. This, **4f** has drug-likeness with the bioavailability score of 0.55. This drug likeness data of **4f** makes it a good drug candidate. Furthermore, other parameters like molecular weight (MW), topological surface area (TPSA), molar refractivity (MR), rotational bond (RB), hydrogen bond donor and acceptors lay in the acceptable range. Other than that, important physicochemical data is indicated in Table 3.

Table 3 Predicted physicochemical properties of **4f** with various filters for drug-likeness[a]

Comp.	MW	RB	HBA	HBD	MR	TPSA	X log *P*	W log *P*	M log *P*	NR	NC	NH	Atom
4f	562.54	10	8	3	151.21	110.17	3.74	4.91	3.32	5	29	12	66

Lipinski filter	Ghose filter	Veber filter	Egan filter	Muegge filter
MW ≤ 500	160 ≤ MW ≤ 480	RB ≤ 10	W log *P* ≤ 5.88	200 ≤ MW ≤ 600
M log *P* ≤ 4.15	−0.4 ≤ W log *P* ≤ 5.6	TPSA ≤ 140	TPSA ≤ 131.6	−2X log *P* ≤ 5; TPSA ≤ 150
HBA ≤ 10	40 ≤ MR ≤ 130			NR ≤ 7; NC > 4; NH > 1; RB ≤ 15; HBA ≤ 10; HBD ≤ 5
HBD ≤ 5	20 ≤ atoms ≤ 70			

[a] Abbreviation: MW: molecular weight; RB: rotational bond; HBA: H-bond acceptor; HBD: H-bond donor; MR: molecular refractivity; TPSA: topological polar surface area; NR: no. of rings; NC: no. of carbon; NH: no. of heteroatoms.

3 Conclusion

A series of benzyloxy derivatives of DHPM was synthesised using a multicomponent reaction. Lanthanum triflate catalyzed reaction gave good to excellent yield within 1–1.5 h. The advantages of this protocol include good to high yields, operational simplicity, simple filtration and needing no extraction or separation by column chromatography is necessary. Out of the series we identified **4f** with the most potent anti-cancer activity in a diverse set of cancer cell lines including primary patient-derived cells. Furthermore, in combination with brain-penetrant small molecule kinase and proteasome inhibitors, **4f** induced potent cytostatic activity and cell cycle impediment which attests for further medicinal chemistry and development of the benzyloxy derivatives of DHPM backbone. Interestingly, treating patient derived glioma stem 3D neurospheres with **4f** significantly reduced neurosphere diameter (Fig. 5), this suggesting potent anti-glioma activity in stem-like organoid models. Furthermore, **4f** exhibited a remarkable potency in combination with EGFR-mutant targeting osimertinib. Although kinase inhibitory activity (ESI Fig. S2†) or apoptosis (ESI Fig. S1†) were not observed for **4f**, the data do suggest that a future *in vivo* bioavailable derivative of **4f** could be used as a combination with osimertinib to target cancers with mutated/amplified EGFR. Both osimertinib and marizomib are covalent inhibitors and represent a paradigm shift toward cancer therapeutics. The ability of our drug to efficiently combine with covalent inhibitor provides an impetus toward further SAR and congener exploration to improve the DHPM backbone for clinical readiness. Compound **4f** shows the most promising drug candidate due to its favorable drug-likeness and *in silico* ADMET properties. Therefore, this study establishes a novel synthetic scheme which will allow for the development of future clinically relevant anti-cancer molecules which can be used in combination with specific drugs targeting EGFR mutated cancers.

4 Experimental

4.1 General

All chemicals were purchased from commercially available sources and used without further purification. Melting points were determined by the open capillary tube method and are uncorrected. ^{1}H NMR and ^{13}C{1H} NMR, HSQC, and HMBC spectral analysis were recorded on BRUKER AVANCE II 600 NMR Spectrometer equipped with cryogenic TCI probe using DMSO-d_6 as the solvents. Abbreviation used for NMR signal: s = Singlet, d = Doublet, t = triplet, dd = double doublet m = Multiplet. The chemical shifts are expressed in parts per million and coupling constants (*J*) are provided in Hertz.

4.2 General procedure for the synthesis of spiroxindoles 4(a–t)

A mixture of 1 mmol 4-((1-benzyl-1*H*-1,2,3-triazole-4-yl)methoxy) benzaldehyde **1(a–c)**, 1.1 mmol of acetoacetenilide derivatives **2(a–k)**, and 1.2 mmol urea derivative **3(a–b)** was added to a 50 ml round bottom flask with 0.5 ml ethanol and 0.1 mmol (10 mol%) lanthanum triflate. It was stirred at 100 °C for 35 min. Within this time, the reaction mixture solidified or became sticky, and then 0.5 ml more ethanol was added and stirred for the required time, as mentioned in Table 2. Next, 5 ml more ethanol was added and cooled to room temperature. The progress of the reaction was monitored by TLC. After completion of the reaction, the reaction mixture was poured slowly into 20 ml ice-cold water with stirring and kept still until the precipitation of the product was completed. The crude product was filtered and washed with 20% aqueous solution of ethanol (5 ml × 3). Products were recrystallized from 6 ml ethanol.

4.2.1 4-(4-((1-Benzyl-1*H*-1,2,3-triazol-4-yl)methoxy)phenyl)-6-methyl-2-oxo-*N*-phenyl-1,2,3,4-tetrahydropyrimidine-5-carboxamide (4a). White solid (0.482 g, 97%), mp: 190–200 °C; ^{1}H NMR (600 MHz, DMSO-d_6) δ: 3.48 (s, 3H), 6.85 (d, J = 7.2 Hz, 2H), 6.88 (t, J = 7.8 Hz, 1H), 7.03 (d, J = 7.8 Hz, 1H), 7.18 (t, J = 7.8 Hz, 1H), 7.43 (NH_2, 2H), 7.44 (t, J = 7.8 Hz, 1H), 7.58 (d, J = 8.4 Hz, 1H), 7.751–7.739 (t, J = 8.4 Hz, 1H), 8.074 (d, J = 8.4 Hz, 1H), 10.53 (NH, 1H); ^{13}C{^{1}H} NMR (151 MHz, DMSO-d_6) δ: 16.93 (CH_3), 52.12 (–CH–), 54.35 (CH_2), 60.96 (CH_2), 105.47, 114.45, 119.47, 122.92, 124.48, 127.40, 128.37, 128.65, 135.87, 136.72, 138.20, 139.15, 142.93, 152.44 (C=O), 157.20 (C–O–), 165.23 (C=O); MS (ESI-TOF) *m*/*z* calcd for $C_{28}H_{25}ClN_6O_3$ $(M + H)^+$: 494.21, found: 495.25.

4.2.2 4-(4-((1-Benzyl-1*H*-1,2,3-triazol-4-yl)methoxy)phenyl)-*N*-(2-chlorophenyl)-6-methyl-2-oxo-1,2,3,4-tetrahydropyrimidine-5-carboxamide (4b). White solid (0.469 g,

89%), mp: 118–120 °C; ^{1}H NMR (600 MHz, DMSO-d$_6$) δ: 2.12 (s, 3H), 5.07 (s, 2H), 5.28 (d, J = 2.8 Hz, 1H), 5.57 (s, 2H), 6.97 (d, j = 8.4 Hz, 2H), 7.10 (t, j = 1.6 Hz and 17.2 Hz, A–H), 7.39–7.20 (m, 10H), 7.45 (d, J = 1.6 Hz and 9.6 Hz), 7.57 (s, 1H), 8.26 (s, 1H), 8.78 (d, j = 2 Hz, 1H), 8.94 (s, 1H); ^{13}C{^{1}H} NMR (151 MHz, DMSO-d$_6$) δ: 17.82 (CH$_3$), 53.35 (–CH–), 54.83 (CH$_2$), 61.57 (CH$_2$), 104.60, 115.12, 125.23, 126.81, 127.19, 128.04, 128.38, 128.52, 128.71, 129.32, 129.87, 135.76, 136.57, 136.92, 141.13, 143.51, 15.92 (C=O), 157.97 (C–O–), 165.73 (C=O); MS (ESI-TOF) m/z calcd for $C_{28}H_{25}ClN_6O_3$ (M + H)$^+$: 528.17, found: 529.03.

4.2.3 4-(4-((1-Benzyl-1*H*-1,2,3-triazol-4-yl)methoxy)phenyl)-*N*-(3-chlorophenyl)-6-methyl-2-oxo-1,2,3,4-tetrahydropyrimidine-5-carboxamide (4c). White solid (0.475 g, 90%), mp: 122–124 °C; ^{1}H NMR (600 MHz, DMSO-d$_6$) δ: 2.00 (s, 3H), 5.04 (s, 2H), 5.33 (dd, j = 2.8 Hz, 1H), 5.55 (s, 2H), 6.93 (d, J = 8.8 Hz, 2H), 7.01 (dd, J = 1.6 Hz and 9.6 Hz, 1H), 7.14 (d, J = 8.8 Hz, 2H), 7.21–7.35 (m, 7H), 7.43 (dd, J = 1.6 Hz and 9.6 Hz, 1H), 7.55 (t, J = 2.4 Hz, 1H), 7.73 (t, J = 2 Hz, 1H), 8.24 (s, 1H), 9.70 (s, 1H); ^{13}C{^{1}H} NMR (151 MHz, DMSO-d$_6$) δ: 17.66 (CH$_3$), 53.34 (–CH–), 54.81 (CH$_2$), 61.54 (CH$_2$), 105.62, 115.09, 118.34, 119.39, 123.19, 125.20, 128.03, 128.51, 128.70, 129.31, 130.76, 133.39, 136.56, 137.28, 139.87, 141.32, 143.52 (C=O), 157.85 (–C–O–), 166.13 (C=O); MS (ESI-TOF) m/z calcd for $C_{28}H_{25}ClN_6O_3$ (M + H)$^+$: 528.16, found: 529.01.

4.2.4 4-(4-((1-Benzyl-1*H*-1,2,3-triazol-4-yl)methoxy)phenyl)-*N*-(4-chlorophenyl)-6-methyl-2-oxo-1,2,3,4-tetrahydropyrimidine-5-carboxamide (4d). White solid (0.480 g, 91%), mp: 128–130 °C; ^{1}H NMR (600 MHz, DMSO-d$_6$) δ: 1.99 (s, 3H), 5.04 (s, 2H), 5.31 (d, J = 2.8 Hz, 1H), 5.55 (s, 2H), 6.93, (d, J = 8 Hz, 2H), 7.14 (d, J = 8 Hz, 2H), 7.24–7.35 (m, 7H), 7.55 (d, J = 8 Hz, 3H), 8.23 (s, 1H), 8.72 (s, 1H), 9.62 (s, 1H); ^{13}C{^{1}H} NMR (151 MHz, DMSO-d$_6$) δ: 17.61 (CH$_3$), 53.35 (–CH–), 54.87 (CH$_2$), 61.54 (CH$_2$), 105.77, 115.08, 121.56, 125.20, 127.09, 128.00, 128.51, 128.70, 128.95, 129.32, 136.55, 137.30, 138.78, 139.49, 153.02 (C=O), 157.05 (C–O), 165.94 (C=O); MS (ESI-TOF) m/z calcd for $C_{28}H_{25}ClN_6O_3$ (M + H)$^+$: 528.16, found: 529.00.

4.2.5 4-(4-((1-Benzyl-1*H*-1,2,3-triazol-4-yl)methoxy)phenyl)-*N*-(4-fluorophenyl)-6-methyl-2-oxo-1,2,3,4-tetrahydropyrimidine-5-carboxamide (4e). Light brown (0.451 g, 88%), mp: 134–136 °C; ^{1}H NMR (600 MHz, DMSO-d$_6$) δ: 2.00 (s, 3H), 5.05 (s, 2H), 5.31 (d, J = 2.8 Hz, 1H), 5.56 (s, 2H), 6.94, (d, J = 8 Hz, 2H), 7.05 (t, J = 8 Hz, 2H), 7.15 (t, j = 8 Hz, 2H), 7.26–7.35 (m, 5H), 7.53 (d, J = 8 Hz, 3H), 8.23 (s, 1H), 8.69 (s, 1H), 9.55 (s, 1H); ^{13}C{^{1}H} NMR (151 MHz, DMSO-d$_6$) δ: 17.58 (CH$_3$), 53.35 (–CH–), 54.92 (CH$_2$), 61.54 (CH$_2$), 105.89, 115.08, 115.49, 115.71, 121.78, 121.85, 125.29, 128.71, 128.03, 128.52, 128.71, 129.32, 136.16, 136.55, 137.32, 139.03, 143.54, 153.08, 157.25, 157.84 (C=O), 159.64 (C–O), 165.78 (C=O); MS (ESI-TOF) m/z calcd for $C_{28}H_{25}FN_6O_3$ (M + H)$^+$: 512.19, found: 513.08.

4.2.6 4-(4-((1-Benzyl-1*H*-1,2,3-triazol-4-yl)methoxy)phenyl)-6-methyl-2-oxo-*N*-(3-(trifluoromethyl)phenyl)-1,2,3,4-tetrahydropyrimidine-5-carboxamide (4f). Light brown (0.511 g, 91%), mp: 230–232 °C; ^{1}H NMR (600 MHz, DMSO-d$_6$) δ: 2.04 (s, 3H), 5.05 (s, 2H), 5.35 (d, J = 2.8 Hz, 1H), 5.56 (s, 2H), 6.94, (d, J = 8 Hz, 2H), 7.16 (d, J = 8 Hz, 2H), 7.26–7.35 (m, 6H), 7.45 (t, J = 8 Hz, 1H), 7.60 (s, 1H), 7.75 (d, J = 8 Hz, 1H), 8.02 (s, 1H), 8.23 (s, 1H), 8.79 (s, 1H), 9.81 (s, 1H); ^{13}C{^{1}H} NMR (151 MHz, DMSO-d$_6$) δ: 17.70 (CH$_3$), 53.35 (–CH–), 54.76 (CH$_2$), 61.54 (CH$_2$), 105.45, 115.13, 115.98, 119.84, 123.49, 125.18, 128.03, 128.51, 128.6, 129.31, 130.31, 13.55, 137.27, 140.26, 143.53, 153.00 (C=O), 157.89 (C–O), 166.29 (C=O); MS (ESI-TOF) m/z calcd for $C_{29}H_{25}F_3N_6O_3$ (M + H)$^+$: 562.19, found: 563.01.

4.2.7 4-(4-((1-Benzyl-1*H*-1,2,3-triazol-4-yl)methoxy)phenyl)-6-methyl-2-oxo-*N*-(*o*-tolyl)-1,2,3,4-tetrahydropyrimidine-5-carboxamide (4g). White solid (0.442 g, 87%), mp: 200–202 °C; ^{1}H NMR (600 MHz, DMSO-d$_6$) δ: 2.04 (s, 3H), 5.05 (s, 2H), 5.35 (d, J = 2.8 Hz, 1H), 5.56 (s, 2H), 6.94, (d, J = 8 Hz, 2H), 7.16 (d, J = 8 Hz, 2H), 7.26–7.35 (m, 6H), 7.45 (t, J = 8 Hz, 1H), 8.02 (s, 1H), 8.79 (s, 1H), 9.81 (s, 1H); ^{13}C{^{1}H} NMR (151 MHz, DMSO-d$_6$) δ: 17.65 (CH$_3$), 18.34, (CH$_3$), 53.36 (–CH–), 55.22 (CH$_2$), 61.59 (CH$_2$), 105.36, 115.04, 125.21, 125.84, 126.30, 128.39, 129.33, 130.9, 133.43, 136.56, 137.08, 139.05, 143.55, 153.93 (C=O), 157.92 (–CH–), 165.72 (C=O); MS (ESI-TOF) m/z calcd for $C_{29}H_{28}N_6O_3$ (M + H)$^+$: 508.22, found: 509.10.

4.2.8 4-(4-((1-Benzyl-1*H*-1,2,3-triazol-4-yl)methoxy)phenyl)-6-methyl-2-oxo-*N*-(*p*-tolyl)-1,2,3,4-tetrahydropyrimidine-5-carboxamide (4h). White solid (0.438 g, 86%), mp: 208–210 °C; ^{1}H NMR (600 MHz, DMSO-d$_6$) δ: 1.99 (s, 3H), 2.18 (s, 3H), 5.05 (s, 2H), 5.31 (d, J = 3.2 Hz, 1H), 5.55 (s, 2H), 6.93, (d, J = 8 Hz, 2H),7.00 (d, J = 8 Hz, 2H), 7.16 (d, J = 8 Hz, 2H), 7.26–7.35 (m, 5H), 7.39 (d, J = 8 Hz, 1H), 7.50 (s, 1H), 8.23 (s, 1H), 8.65 (s, 1H), 9.41 (s, 1H); ^{13}C{^{1}H} NMR (151 MHz, DMSO-d$_6$) δ: 17.55 (CH$_3$), 20.96 (CH$_3$), 53.35 (–CH–), 54.97 (CH$_2$) 61.55 (CH$_2$), 106.17, 115.05, 120.11, 125.19, 128.05, 128.51, 128.71, 129.32, 129.41, 132.48, 136.55, 137.29, 137.37, 138.60, 143.54, 153.13 (C=O), 157.82 (C–O), 165.68 (C=O); MS (ESI-TOF) m/z calcd for $C_{29}H_{28}N_6O_3$ (M + H)$^+$: 508.22, found: 509.10.

4.2.9 4-(4-((1-Benzyl-1*H*-1,2,3-triazol-4-yl)methoxy)phenyl)-*N*-(2-methoxyphenyl)-6-methyl-2-oxo-1,2,3,4-tetrahydropyrimidine-5-carboxamide (4i). White solid (0.477 g, 91%), mp: 220–222 °C; ^{1}H NMR (600 MHz, DMSO-d$_6$) δ: 2.15 (s, 3H), 3.60 (s, 3H), 5.07 (d, J = 12 Hz, 2H), 5.15 (d, J = 12 Hz, 2H), 5.56 (s, 2H), 6.81 (t, J = 8 Hz, 2H),7.00–7.16 (m, 8H), 7.55 (s, 1H), 7.83 (d, J = 8 Hz, 1H), 8.11 (s, 1H), 8.26 (s, 1H), 8.84 (s, 1H); ^{13}C{^{1}H} NMR (151 MHz, DMSO-d$_6$) δ: 17.82 (CH$_3$), 53.37 (CH$_3$), 54.93 (–CH–), 56.03 (CH$_2$), 61.57 (CH$_2$), 104.31, 111.36, 115.29, 120.76, 121.72, 124.51, 125.23, 127.97, 128.54, 128.72, 129.33, 136.54, 142.34, 143.53, 149.79 (C=O), 152.69 (C–O), 158.18 (C–O), 165.06 (C=O).; MS (ESI-TOF) m/z calcd for $C_{29}H_{28}N_6O_4$ (M + H)$^+$: 524.22, found: 525.03.

4.2.10 4-(4-((1-Benzyl-1*H*-1,2,3-triazol-4-yl)methoxy)phenyl)-*N*-(4-methoxyphenyl)-6-methyl-2-oxo-1,2,3,4-tetrahydropyrimidine-5-carboxamide (4j). White solid (0.467 g, 89%), mp: 226–228 °C; ^{1}H NMR (600 MHz, DMSO-d$_6$) δ: 1.19 (s, 3H), 3.65 (s, 3H), 5.05 (s, 2H), 5.31 (s, 2H), 5.55 (s, 1H), 6.78, (d, J = 8 Hz, 2H), 6.94 (d, J = 8 Hz, 2H), 7.15 (d, J = 8 Hz, 2H), 7.26–7.35 (m, 6H), 7.41 (d, J = 8 Hz, 1H), 7.50 (s, 1H), 8.23 (s, 1H), 8.65 (s, 1H), 9.37 (s, 1H); ^{13}C{^{1}H} NMR (151 MHz, DMSO-d$_6$) δ: 17.54 (CH$_3$), 53.35 (CH$_3$), 54.98 (–CH–), 55.67 (CH$_2$), 67.55 (CH$_2$), 106.18, 114.17, 118.05, 121.67, 125.19, 128.05, 128.51, 128.71, 129.32, 132.92, 136.55, 137.38, 138.35, 143.57, 153.16 (C=O), 155.67 (C–O), 157.82 (C–O), 168.47 (C=O); MS (ESI-TOF) m/z calcd for $C_{29}H_{28}N_6O_4$ (M + H)$^+$: 524.22, found: 525.08.

4.2.11 4-(4-((1-Benzyl-1*H*-1,2,3-triazol-4-yl)methoxy) phenyl)-6-methyl-*N*-phenyl-2-thioxo-1,2,3,4-tetrahydropyrimidine-5-carboxamide (4k). White solid (0.403 g, 79%), mp: 180–182 °C; ^{1}H NMR (600 MHz, DMSO-d$_6$) δ: 2.03 (s, 3H), 5.06 (s, 2H), 5.32 (d, J = 3.2 Hz, 1H), 5.56 (s, 2H), 6.98, (td, J = 2 Hz and 17.2 Hz, 3H), 7.14 (d, J = 8 Hz, 2H), 7.26–7.35 (m, 7H), 7.51 (d, J = 8 Hz, 2H), 8.23 (s, 1H), 9.38 (s, 1H), 9.68 (s, 1H), 9.95 (s, 1H); ^{13}C{^{1}H} NMR (151 MHz, DMSO-d$_6$) δ: 17.03 (CH_3), 53.36 (–CH–), 55.01 (CH_2), 61.58 (CH_2), 107.89, 115.22, 120.16, 123.86, 125.21, 128.24, 128.51, 128.71, 129.12, 129.32, 135.94, 136.08, 136.55, 139.54, 143.49, 158.11 (C=O), 165.53 (C–O), 174.38 (C=S); MS (ESI-TOF) m/z calcd for $C_{28}H_{26}N_6O_2S$ (M + H)$^+$: 445.1067, found: 445.1081.

4.2.12 4-(4-((1-Benzyl-1*H*-1,2,3-triazol-4-yl)methoxy) phenyl)-*N*-(2-chlorophenyl)-6-methyl-2-thioxo-1,2,3,4-tetrahydropyrimidine-5-carboxamide (4l). White solid (0.479 g, 94%), mp: 116–118 °C; ^{1}H NMR (600 MHz, DMSO-d$_6$) δ: 1.08 (t, J = 6.6 Hz, 3H), 4.13 (q, J = 3.72 Hz, 2H), 4.30 (dd, J = 2.64 Hz and 16.56 Hz, 1H), 4.46 (dd, J = 2.46 Hz and 15.51 Hz, 1H), 5.21 (d, J = 10.5 Hz, 1H), 5.49 (d, J = 17.28 Hz, 1H), 5.87 (tt, J = 4.14 Hz and 12 Hz, 1H), 6.95 (d, J = 8.4 Hz, 1H), 7.32 (t, J = 8.4 Hz, 1H), 7.45 (t, J = 7.2 Hz, 1H), 7.61 (NH_2, 2H), 7.65 (d, J = 8.4 Hz, 1H), 7.77 (t, J = 7.8 Hz, 1H), 8.10 (d, J = 8.4 Hz, 1H); ^{13}C{^{1}H} NMR (151 MHz, DMSO-d$_6$) δ: 16.57 (CH_3), 52.74 (–CH–), 54.34 (CH_2), 61.00 (CH_2), 105.99, 114.60, 124.52, 126.51, 126.79, 127.20, 127.75, 127.85, 128.04, 128.66, 129.29, 134.80, 135.16, 135.87, 136.91, 142.85, 157.56 (C=O), 164.87 (C–O), 173.68 (C=S); MS (ESI-TOF) m/z calcd for $C_{28}H_{25}ClN_6O_2S$ (M + H)$^+$: 510.18, found: 511.06.

4.2.13 4-(4-((1-Benzyl-1*H*-1,2,3-triazol-4-yl)methoxy) phenyl)-*N*-(3-chlorophenyl)-6-methyl-2-thioxo-1,2,3,4-tetrahydropyrimidine-5-carboxamide (4m). Light brown(0.500 g, 92%), mp: 120–122 °C; ^{1}H NMR (600 MHz, DMSO-d$_6$) δ: 2.04 (s, 3H), 5.06 (s, 2H), 5.32 (d, J = 3.2 Hz, 1H), 5.56 (s, 2H), 6.98, (d, J = 8 Hz, 2H), 7.04 (d, J = 8 Hz, 1H), 7.14 (d, J = 8 Hz, 2H), 7.26–7.35 (m, 6H), 7.42 (d, J = 8 Hz, 2H), 7.72 (s, 1H), 8.23 (s, 1H), 9.44 (s, 1H), 9.84 (s, 1H), 10.00 (s, 1H); ^{13}C{^{1}H} NMR (151 MHz, DMSO-d$_6$) δ: 17.09 (CH_3), 53.36 (–CH–), 54.89 (CH_2), 61.57 (CH_2), 107.41, 115.26, 118.43, 119.60, 123.51, 125.21, 128.21, 128.51, 128.71, 129.32, 130.86, 133.47, 136.03, 136.55, 136.82, 141.01, 143.47, 158.14(C=O), 165.79 (C–O), 174.42 (C=S); MS (ESI-TOF) m/z calcd for $C_{28}H_{25}ClN_6O_2S$ (M + H)$^+$: 544.14, found: 544.98.

4.2.14 4-(4-((1-Benzyl-1*H*-1,2,3-triazol-4-yl)methoxy) phenyl)-*N*-(4-chlorophenyl)-6-methyl-2-thioxo-1,2,3,4-tetrahydropyrimidine-5-carboxamide (4n). Light brown (0.484 g, 89%), mp: 126–128 °C; ^{1}H NMR (600 MHz, DMSO-d$_6$) δ: 2.04 (s, 3H), 5.06 (s, 2H), 5.32 (d, J = 3.2 Hz, 1H), 5.56 (s, 2H), 6.96 (d, J = 8 Hz, 2H), 7.14 (d, J = 8 Hz, 2H), 7.26–7.35 (m, 7H), 7.55 (d, J = 8 Hz, 2H), 8.23 (s, 2H), 9.44 (s, 1H), 9.84 (s, 1H), 9.98 (s, 1H); ^{13}C{^{1}H} NMR (151 MHz, DMSO-d$_6$) δ: 17.07(CH_3), 53.36 (–CH–), 54.94 (CH_2), 61.57 (CH_2), 107.57, 115.24, 121.66, 125.21, 127.40, 128.21, 128.56, 129.25, 129.32, 136.04, 136.47, 136.59, 138.49, 143.47, 158.12 (C=O), 165.61 (C–O), 174.41 (C=S); MS (ESI-TOF) m/z calcd for $C_{28}H_{25}ClN_6O_2S$ (M + H)$^+$: 544.14, found: 544.97.

4.2.15 4-(4-((1-Benzyl-1*H*-1,2,3-triazol-4-yl)methoxy) phenyl)-*N*-(4-fluorophenyl)-6-methyl-2-thioxo-1,2,3,4-tetrahydropyrimidine-5-carboxamide (4o). White solid (0.502 g, 95%), mp: 232–234 °C; ^{1}H NMR (600 MHz, DMSO-d$_6$) δ: 2.04 (s, 3H), 5.06 (s, 2H), 5.32 (d, J = 3.2 Hz, 1H), 5.56 (s, 2H), 6.96 (d, J = 8 Hz, 2H), 7.04 (d, J = 8 Hz, 1H), 7.14 (d, J = 8 Hz, 2H), 7.26–7.35 (m, 6H), 7.55 (t, J = 8 Hz, 2H), 8.23 (s, 1H), 9.40 (t, J = 2 Hz, 1H), 9.84 (s, 1H), 9.98 (s, 1H); ^{13}C{^{1}H} NMR (151 MHz, DMSO-d$_6$) δ: 17.04 (CH_3), 53.36 (–CH–), 54.98 (CH_2), 61.57 (CH_2), 107.69, 115.23, 115.58, 118.79, 121.89, 121.97, 125.21, 128.22, 128.51, 128.71, 129.32, 135.89, 136.07, 136.57, 143.48, 157.40, 158.12, 159.78(C=O), 165.44 (C–O), 174.40 (C=S); MS (ESI-TOF) m/z calcd for $C_{28}H_{25}FN_6O_2S$ (M + H)$^+$: 528.17, found: 529.02.

4.2.16 4-(4-((1-Benzyl-1*H*-1,2,3-triazol-4-yl)methoxy) phenyl)-6-methyl-2-thioxo-*N*-(3-(trifluoromethyl)phenyl)-1,2,3,4-tetrahydropyrimidine-5-carboxamide (4p). White solid (0.491 g, 85%), mp: 250–252 °C; ^{1}H NMR (600 MHz, DMSO-d$_6$) δ: 2.04 (s, 3H), 5.06 (s, 2H), 5.32 (d, J = 3.2 Hz, 1H), 5.56 (s, 2H), 6.96 (d, J = 8 Hz, 2H), 7.14 (d, J = 8 Hz, 2H), 7.26–7.35 (m, 6H), 7.47 (t, J = 8 Hz, 1H), 7.75 (t, J = 8 Hz, 2H), 8.02 (s, 1H), 8.23 (s, 1H), 9.40 (t, J = 2 Hz, 1H), 9.98 (s, 1H), 10.00 (s, 1H); ^{13}C{^{1}H} NMR (151 MHz, DMSO-d$_6$) δ: 17.40 (CH_3), 53.35 (–CH–), 54.82 (CH_2), 61.57 (CH_2), 107.20, 115.27, 116.08, 120.13, 123.60, 125.21, 128.23, 128.51, 128.70, 129.31, 130.39, 136.01, 136.55, 137.21, 140.34, 143.47, 158.16 (C=O), 165.97 (C–O), 174.43 (C=S); MS (ESI-TOF) m/z calcd for $C_{29}H_{25}F_3N_6O_2S$ (M + H)$^+$: 578.17, found: 579.01.

4.2.17 4-(4-((1-Benzyl-1*H*-1,2,3-triazol-4-yl)methoxy) phenyl)-6-methyl-2-thioxo-*N*-(*o*-tolyl)-1,2,3,4-tetrahydropyrimidine-5-carboxamide (4q). White solid (0.451 g, 86%), mp: 190–192 °C; ^{1}H NMR (600 MHz, DMSO-d$_6$) δ: 1.87 (s, 3H), 2.04 (s, 3H) 5.09 (s, 2H), 5.32 (d, J = 3.2 Hz, 1H), 5.56 (s, 2H), 6.96–7.14 (m, 8H), 7.19 (t, J = 8 Hz, 2H), 7.47 (t, J = 8 Hz, 1H), 7.75 (t, J = 8 Hz, 2H), 8.02 (s, 1H), 8.23 (s, 1H), 9.40 (t, J = 2 Hz, 1H), 9.98 (s, 1H), 10.00 (s, 1H); ^{13}C{^{1}H} NMR (151 MHz, DMSO-d$_6$) δ: 17.10 (CH_3), 18.36 (CH_3), 53.38 (–CH–), 55.29 (CH_2), 61.61 (CH_2), 107.36, 115.18, 125.28, 126.09, 126.39, 128.53, 128.57, 128.73, 129.34, 130.77, 133.54, 135.91, 136.02, 136.55, 136.74, 143.49, 158.18 (C=O), 165.46 (C–O), 174.55 (C=S); MS (ESI-TOF) m/z calcd for $C_{29}H_{28}N_6O_2S$ (M + H)$^+$: 524.20, found: 525.03.

4.2.18 4-(4-((1-Benzyl-1*H*-1,2,3-triazol-4-yl)methoxy) phenyl)-6-methyl-2-thioxo-*N*-(*p*-tolyl)-1,2,3,4-tetrahydropyrimidine-5-carboxamide (4r). White solid (0.461 g, 88%), mp: 184–186 °C; ^{1}H NMR (600 MHz, DMSO-d$_6$) δ: 2.02 (s, 3H), 2.18 (s, 3H) 5.09 (s, 2H), 5.30 (s, 1H), 5.56 (s, 2H), 6.96 (d, J = 8 Hz, 2H), 7.02 (d, J = 8 Hz, 2H), 7.13 (d, J = 8 Hz, 2H), 7.26–7.35 (m, 6H), 7.39 (d, J = 8 Hz, 1H), 8.23 (s, 1H), 9.36 (s, 1H), 9.59 (s, 1H), 9.98 (s, 1H); ^{13}C{^{1}H} NMR (151 MHz, DMSO-d$_6$) δ: 17.60 (CH_3), 20.97 (CH_3), 53.36 (–CH–), 55.03 (CH_2), 61.57 (CH_2), 107.96, 115.20, 120.19, 125.21, 128.24, 128.51, 128.71, 129.32, 129.48, 132.80, 135.71, 136.10, 136.55, 137.02, 143.49, 158.09 (C=O), 165.31 (C–O), 174.36 (C=S); MS (ESI-TOF) m/z calcd for $C_{29}H_{28}N_6O_2S$ (M + H)$^+$: 524.19, found: 525.03.

4.2.19 4-(4-((1-Benzyl-1*H*-1,2,3-triazol-4-yl)methoxy) phenyl)-*N*-(4-methoxyphenyl)-6-methyl-2-thioxo-1,2,3,4-tetrahydropyrimidine-5-carboxamide (4s). White solid (0.487 g,

90%), mp: 200–202 °C; ^{1}H NMR (600 MHz, DMSO-d_6) δ: 2.16 (s, 3H), 3.63 (s, 3H), 5.09 (s, 2H), 5.22 (d, J = 8 Hz, 2H), 5.56 (s, 2H), 6.96 (dt, J = 1.6 Hz and 16.8 Hz, 1H), 6.98–7.02 (m, 3H), 7.31–7.35 (m, 2H), 7.74 (dd, J = 1.6 Hz and 9.6 Hz, 1H), 8.23 (s, 1H), 8.92 (s, 1H), 9.41 (d, J = 1.6 Hz, 1H), 10.00 (d, J = 1.6 Hz, 1H); ^{13}C{^{1}H} NMR (151 MHz, DMSO-d_6) δ: 17.22 (CH_3), 53.37 (CH_3), 54.94 (–CH–), 56.08 (CH_2), 61.60 (CH_2), 106.42, 111.54, 115.34, 120.74, 122.55, 125.09, 125.23, 127.56, 128.53, 128.72, 129.33, 135.54, 136.54, 138.45, 143.48, 150.36 (C=O), 158.36 (C–O), 164.83 (C–O), 174.02 (C=S); MS (ESI-TOF) m/z calcd for $C_{29}H_{28}N_6O_3S$ (M + H)$^+$: 540.19, found: 541.00.

4.2.20 4-(4-((1-Benzyl-1*H*-1,2,3-triazol-4-yl)methoxy) phenyl)-*N*-(2-methoxyphenyl)-6-methyl-2-thioxo-1,2,3,4-tetrahydropyrimidine-5-carboxamide (4t). White solid (0.475 g, 88%), mp: 204–206 °C; ^{1}H NMR (600 MHz, DMSO-d_6) δ: 2.04 (s, 3H), 3.65 (s, 3H), 5.06 (s, 2H), 5.32 (d, J = 3.2 Hz, 1H), 5.56 (s, 2H), 6.80 (d, J = 8 Hz, 2H), 6.96 (d, J = 8 Hz, 2H), 7.14 (d, J = 8 Hz, 2H), 7.26–7.35 (m, 5H), 7.47 (d, J = 8 Hz, 1H), 8.23 (s, 1H), 9.40 (t, J = 2 Hz, 1H), 9.55 (s, 1H), 9.92 (s, 1H); ^{13}C{^{1}H} NMR (151 MHz, DMSO-d_6) δ: 16.99 (CH_3), 53.36 (CH_3), 55.04 (–CH–), 55.68 (CH_2), 61.58 (CH_2), 107.99, 114.24, 115.20, 121.75, 125.20, 128.24, 128.51, 128.71, 129.33, 132.63, 135.50, 136.11, 136.55, 143.49, 155.84 (C=O), 158.09 (C–O), 165.08 (C–O), 174.34 (C=S); MS (ESI-TOF) m/z calcd for $C_{29}H_{28}N_6O_3S$ (M + H)$^+$: 540.19, found: 541.04.

4.3 Materials and methods

4.3.1 Materials and cell lines. Drugs PI-103 (#A2067-APE), buparlisib (#ORB669009-BOR), abemaciclib (#S5716-SEL), bozitinib (#S6762-SEL), marizomib (#SML1916-100UG), nilotinib (#S1033-SEL), crenolanib (#S2730-SEL), and osimertinib (#S7297-SEsssL) were purchased from Stratech, UK as stated previously.[50] The compounds were dissolved in DMSO to a working stock of 10 mM. Propidium iodide was purchased from Sigma-Millipore. MDA-MB-231 (a triple negative breast cancer epithelial cell line), A549 (a non-small cell lung cancer cell line), HEPG2 (derived from a patient with the hepatocellular carcinoma) and U87 MG (U87) cells were from ATCC. GBM6, GBM120, and GBM22 were acquired from the Brain Tumour PDX National Resource, Mayo Clinic, USA.[20] Insulin and epidermal growth factor were purchased from Sigma Millipore.

4.3.2 Cell culture. Mammalian cells were all grown in a humidified incubator with 5% CO_2 at 37 °C. U87 and HEPG2 cell lines were cultured in Dulbecco's modified Eagle's medium (DMEM, Gibco) supplemented with 10% FBS and 1% penicillin and streptomycin. MDA-MB-231, A549 and primary patient glioblastoma cell lines (GBM6 and GBM22) were cultured in DMEM supplemented with 10% FBS, 1% penicillin and streptomycin, 10 μg ml^{-1} insulin, and 20 ng ml^{-1} hEGF as stated previously.[20] GBM120 cells were cultured in neurosphere media consisting of KnockOut DMEM/F-12 Basal Media supplemented with StemPro NSC SFM Supplement, 10 mg FGF, 10 mg EGF, L-glutamine (Corning #25005CI) 10 ml of 200 mM solution, and 1% penicillin and streptomycin.

4.3.3 Cell viability and apoptosis assays. To measure cell viability, actively proliferating cells were seeded at with an equal number of cells per well. Cell viability assays were carried out with 48–96 h treatment of indicated drugs or DMSO control using CellTiter 96® AQueous Non-Radioactive Cell proliferation assay, adhering to manufacturer instructions. Absorbance was measured using a Tecan multi-well plate reader and data was represented as % viability compared to DMSO treated control as stated previously.[20,51,52] For the assessment of apoptosis, Annexin V-FITC (ab176749; Abcam, Cambridge, UK) was used as stated previously.[53] 16 h post drug treatments, the wells were washed and buffer solution containing Annexin V-FITC diluted as par manufacturer's instructions were added to the wells. The cells were incubated for 90 min prior to imaging. Bright field and fluorescent imaging were taken using a Thermo Scientific EVOS imaging system.

4.3.4 Cell cycle analyses. Cell cycle analyses using propidium iodide and flow cytometry were carried out as described previously.[52,54] Asynchronous GBM6 cells were treated with either DMSO or **4f** at 15 or 25 μM for 16 h. Post treatment, cells were washed with PBS + 1% FBS and resuspended in flow cytometry tubes. Cells were then fixed with 70% ice-cold ethanol and propidium iodide (50 μg ml^{-1}) was added to the cells and incubated in the dark at room temperature (25 °C) for 30 min. The cell populations were then subjected to quantitative measurement of DNA content by flow cytometry using a FACS-Fortessa (BD Biosciences) and cell cycle distribution and the percentage of G_2/M–S–G_1 cells to the total cell events were determined by the BD FACS Diva software. Stacked bar graphs were derived using Graphpad Prism.

4.3.5 Neurosphere formation assay. Neurosphere formation assay was carried out as stated previously.[20] Briefly, GBM120 cells were plated at 4000 cells per well in neurosphere media supplemented with either DMSO, 15 μM and 25 μM of **4f** for 13 days in triplicates. After 13 days, representative images were taken of each well using the Zeiss Axiovert Live microscope. Diameters of the neurospheres were quantified using ImageJ software, and graphs were plotted on GraphPad Prism.

4.3.6 Kinase screen analysis of 4f. Kinase inhibitor specificity profiling assays were carried out at The International Centre for Protein Kinase Profiling (http://www.kinase-screen.mrc.ac.uk/) as stated previously.[20] Briefly, **4f** biochemical kinase inhibitory property was determined against a panel of 139 protein kinases as described previously.[55,56] Protein kinases were assayed *in vitro* with 10 μM final concentration of **4f** and results are presented as a percentage of kinase activity to DMSO control reactions as an average of triplicate reactions in the form of comparative histograms using Adobe Illustrator.

4.3.7 Statistical analysis. All analysis was conducted using Graphpad Prism statistical package and presented as mean ± SD unless otherwise stated. Figure legends contain details of the statistical tests and multiple comparisons conducted throughout. Experiments were repeated 2–3 times with multiple technical replicates for the appropriate statistical tests to be conducted.

4.3.8 *In silico* ADMET prediction. *In silico* ADMET prediction of the synthesized DHPM compound **4f** was accomplished

with the help of the web tool SwissADME[57] (http://www.swissadme.ch/).

Data availability

The data supporting this article have been included as part of the ESI.†

Conflicts of interest

DBU, JN, RMV, SB, and HMP are named inventors on the patent no. 528662 awarded by the government of India on 18th March 2024 pertaining to these reported compounds. No other conflicts of interest reported.

Acknowledgements

DBU, JAM, RMV and HMP are grateful to the department of chemistry, Sardar Patel University for providing lab facilities. DBU is thankful to Knowledge Consortium of Gujarat (KCG), Department of Education, Government of Gujarat, India for SHODH-Scheme of Developing High Quality Research (Student Ref No. 2021016413). JAM is grateful to CSIR, New Delhi, for a CSIR-SRF. SB is funded by the United Kingdom Research and Innovation Future Leader Fellowship MR/W008114/1. VT and SB are funded by the Ninewells Cancer Campaign Cancer Research grant.

References

1 S. Arunkhamkaew, A. Athipornchai, N. Apiratikul, A. Suksamrarn and V. Ajavakom, Novel racemic tetrahydrocurcuminoid dihydropyrimidinone analogues as potent acetylcholinesterase inhibitors, *Bioorg. Med. Chem. Lett.*, 2013, **23**(10), 2880–2882.

2 J. Kim, C. Park, T. Ok, W. So, M. Jo, M. Seo, Y. Kim, J.-H. Sohn, Y. Park, M. K. Ju, J. Kim, S.-J. Han, T.-H. Kim, J. Cechetto, J. Nam, P. Sommer and Z. No, Discovery of 3,4-dihydropyrimidin-2(1H)-ones with inhibitory activity against HIV-1 replication, *Bioorg. Med. Chem. Lett.*, 2012, **22**(5), 2119–2124.

3 S. Shamim, K. M. Khan, U. Salar, F. Ali, M. A. Lodhi, M. Taha, F. A. Khan, S. Ashraf, Z. Ul-Haq, M. Ali and S. Perveen, 5-Acetyl-6-methyl-4-aryl-3,4-dihydropyrimidin-2(1H)-ones: As potent urease inhibitors; synthesis, in vitro screening, and molecular modeling study, *Bioorg. Chem.*, 2018, **76**, 37–52.

4 İ. S. Zorkun, S. Saraç, S. Çelebi and K. Erol, Synthesis of 4-aryl-3,4-dihydropyrimidin-2(1H)-thione derivatives as potential calcium channel blockers, *Bioorg. Med. Chem.*, 2006, **14**(24), 8582–8589.

5 N. C. Desai, S. B. Joshi and K. A. Jadeja, A one-pot multicomponent Biginelli reaction for the preparation of novel pyrimidinthione derivatives as antimicrobial agents, *J. Heterocycl. Chem.*, 2020, **57**(2), 791–795.

6 H. A. Stefani, C. B. Oliveira, R. B. Almeida, C. M. P. Pereira, R. C. Braga, R. Cella, V. C. Borges, L. Savegnago and C. W. Nogueira, Dihydropyrimidin-(2H)-ones obtained by ultrasound irradiation: a new class of potential antioxidant agents, *Eur. J. Med. Chem.*, 2006, **41**(4), 513–518.

7 M. Dubernet, N. Duguet, L. Colliandre, C. Berini, S. Helleboid, M. Bourotte, M. Daillet, L. Maingot, S. Daix, J.-F. Delhomel, L. Morin-Allory, S. Routier and R. Walczak, Identification of New Nonsteroidal RORα Ligands; Related Structure–Activity Relationships and Docking Studies, *ACS Med. Chem. Lett.*, 2013, **4**(6), 504–508.

8 M. Sagha, F. Mousaei, M. Salahi and N. Razzaghi-Asl, Synthesis of new 2-aminothiazolyl/benzothiazolyl-based 3,4-dihydropyrimidinones and evaluation of their effects on adenocarcinoma gastric cell migration, *Mol. Diversity*, 2022, **26**(2), 1039–1051.

9 N. C. Desai, A. R. Trivedi, H. V. Vaghani, H. C. Somani and K. A. Bhatt, Synthesis and biological evaluation of 1,3,4-oxadiazole bearing dihydropyrimidines as potential antitubercular agents, *Med. Chem. Res.*, 2016, **25**(2), 329–338.

10 S. J. Teague, A. M. Davis, P. D. Leeson and T. Oprea, The Design of Leadlike Combinatorial Libraries, *Angew. Chem., Int. Ed.*, 1999, **38**(24), 3743–3748.

11 R. M. Vala, M. G. Sharma, D. M. Patel, A. Puerta, J. M. Padron, V. Ramkumar, R. L. Gardas and H. M. Patel, Synthesis and in vitro study of antiproliferative benzyloxy dihydropyrimidinones, *Arch. Pharm.*, 2021, **354**(6), 2000466.

12 Z. Bidram, H. Sirous, G. A. Khodarahmi, F. Hassanzadeh, N. Dana, A. A. Hariri and M. Rostami, Monastrol derivatives: in silico and in vitro cytotoxicity assessments, *Res. Pharm. Sci.*, 2020, **15**(3), 249–262.

13 A. Castillo and M. J. Justice, The kinesin related motor protein, Eg5, is essential for maintenance of pre-implantation embryogenesis, *Biochem. Biophys. Res. Commun.*, 2007, **357**(3), 694–699.

14 N. Hirokawa, Y. Noda, Y. Tanaka and S. Niwa, Kinesin superfamily motor proteins and intracellular transport, *Nat. Rev. Mol. Cell Biol.*, 2009, **10**(10), 682–696.

15 I. Garcia-Saez, S. DeBonis, R. Lopez, F. Trucco, B. Rousseau, P. Thuéry and F. Kozielski, Structure of human Eg5 in complex with a new monastrol-based inhibitor bound in the R configuration, *J. Biol. Chem.*, 2007, **282**(13), 9740–9747.

16 T. U. Mayer, T. M. Kapoor, S. J. Haggarty, R. W. King, S. L. Schreiber and T. J. Mitchison, Small Molecule Inhibitor of Mitotic Spindle Bipolarity Identified in a Phenotype-Based Screen, *Science*, 1999, **286**(5441), 971–974.

17 D. Russowsky, R. F. S. Canto, S. A. A. Sanches, M. G. M. D'Oca, Â. de Fátima, R. A. Pilli, L. K. Kohn, M. A. Antônio and J. E. de Carvalho, Synthesis and differential antiproliferative activity of Biginelli compounds against cancer cell lines: Monastrol, oxo-monastrol and oxygenated analogues, *Bioorg. Chem.*, 2006, **34**(4), 173–182.

18 V. Tandon, R. M. Vala, A. Chen, R. L. Sah, H. M. Patel, M. C. Pirrung and S. Banerjee, Syrbactin-class dual constitutive-and immuno-proteasome inhibitor TIR-199 impedes myeloma-mediated bone degeneration in vivo, *Biosci. Rep.*, 2022, **42**(2), BSR20212721.

19 S. G. Patel, R. M. Vala, P. J. Patel, D. B. Upadhyay, V. Ramkumar, R. L. Gardas and H. M. Patel, Synthesis, crystal structure and in silico studies of novel 2, 4-dimethoxy-tetrahydropyrimido [4, 5-b] quinolin-6 (7 H)-ones, *RSC Adv.*, 2022, **12**(29), 18806–18820.

20 R. M. Vala, V. Tandon, L. G. Nicely, L. Guo, Y. Gu, S. Banerjee and H. M. Patel, Synthesis of N-(4-chlorophenyl) substituted pyrano[2,3-c]pyrazoles enabling PKBβ/AKT2 inhibitory and in vitro anti-glioma activity, *Ann. Med.*, 2022, **54**(1), 2549–2561.

21 S. G. Patel, A. González-Bakker, R. M. Vala, P. J. Patel, A. Puerta, A. Malik, R. K. Sharma, J. M. Padrón and H. M. Patel, Microwave-assisted multicomponent synthesis of antiproliferative 2,4-dimethoxy-tetrahydropyrimido[4,5-b]quinolin-6(7H)-ones, *RSC Adv.*, 2022, **12**(47), 30404–30415.

22 D. B. Upadhyay, J. A. Mokariya, P. J. Patel, S. G. Patel, A. Das, A. Nandi, J. Nogales, N. More, A. Kumar, D. P. Rajani, M. Narayan, J. Kumar, S. Banerjee, S. K. Sahoo and H. M. Patel, Indole clubbed 2,4-thiazolidinedione linked 1,2,3-triazole as a potent antimalarial and antibacterial agent against drug-resistant strain and molecular modeling studies, *Arch. Pharm.*, 2024, e2300673.

23 J. A. Mokariya, D. P. Rajani and M. P. Patel, 1,2,4-Triazole and benzimidazole fused dihydropyrimidine derivatives: Design, green synthesis, antibacterial, antitubercular, and antimalarial activities, *Arch. Pharm.*, 2023, **356**(4), e2200545.

24 J. A. Mokariya, A. G. Kalola, P. Prasad and M. P. Patel, Simultaneous ultrasound- and microwave-assisted one-pot 'click' synthesis of 3-formyl-indole clubbed 1,2,3-triazole derivatives and their biological evaluation, *Mol. Diversity*, 2022, **26**(2), 963–979.

25 D. P. Vala, R. M. Vala and H. M. Patel, Versatile Synthetic Platform for 1,2,3-Triazole Chemistry, *ACS Omega*, 2022, **7**(42), 36945–36987.

26 N. Anand, K. K. G. Ramakrishna, M. P. Gupt, V. Chaturvedi, S. Singh, K. K. Srivastava, P. Sharma, N. Rai, R. Ramachandran and A. K. Dwivedi, Identification of 1-[4-benzyloxyphenyl-but-3-enyl]-1 H-azoles as new class of antitubercular and antimicrobial agents, *ACS Med. Chem. Lett.*, 2013, **4**(10), 958–963.

27 S. Emami, M. Kazemi-Najafabadi, S. Pashangzadeh, A. Foroumadi, M. A. Faramarzi, N. Samadi, M. Falahati, R. Fateh and M. Ashrafi-Khozani, Synthesis and Antifungal Activity of 1-[(2-Benzyloxy) Phenyl]-2-(Azol-1-yl) Ethanone Derivatives: Exploring the Scaffold Flexibility, *Chem. Biol. Drug Des.*, 2011, **78**(6), 979–987.

28 B. S. Kumar, A. Kumar, J. Singh, M. Hasanain, A. Singh, K. Fatima, D. K. Yadav, V. Shukla, S. Luqman and F. Khan, Synthesis of 2-alkoxy and 2-benzyloxy analogues of estradiol as anti-breast cancer agents through microtubule stabilization, *Eur. J. Med. Chem.*, 2014, **86**, 740–751.

29 A. M. King, X.-F. Yang, Y. Wang, E. T. Dustrude, C. Barbosa, M. R. Due, A. D. Piekarz, S. M. Wilson, F. A. White and C. Salomé, Identification of the benzyloxyphenyl pharmacophore: a structural unit that promotes sodium channel slow inactivation, *ACS Chem. Neurosci.*, 2012, **3**(12), 1037–1049.

30 X. Dou, D. Nath, H. Shin, E. Nurmemmedov, P. C. Bourne, J.-X. Ma and A. S. Duerfeldt, Evolution of a 4-benzyloxy-benzylamino chemotype to provide efficacious, potent, and isoform selective PPARα agonists as leads for retinal disorders, *J. Med. Chem.*, 2020, **63**(6), 2854–2876.

31 S. T. Sudevan, T. M. Rangarajan, A. G. Al-Sehemi, A. S. Nair, V. P. Koyiparambath and B. Mathew, Revealing the role of the benzyloxy pharmacophore in the design of a new class of monoamine oxidase-B inhibitors, *Arch. Pharm.*, 2022, **355**(8), 2200084.

32 D. B. Upadhyay, R. M. Vala, J. Nogales, S. Banerjee and H. M. Patel, *A tetrahydopyrimidinecarboxamide derivatives*, 2024, p. 528662.

33 M. M. Alam, 1,2,3-Triazole hybrids as anticancer agents: A review, *Arch. Pharm.*, 2022, **355**(1), 2100158.

34 K. Lal and P. Yadav, Recent advancements in 1, 4-disubstituted 1H-1, 2, 3-triazoles as potential anticancer agents, *Anti-Cancer Agents Med. Chem.*, 2018, **18**(1), 21–37.

35 J. Akhtar, A. A. Khan, Z. Ali, R. Haider and M. Shahar Yar, Structure-activity relationship (SAR) study and design strategies of nitrogen-containing heterocyclic moieties for their anticancer activities, *Eur. J. Med. Chem.*, 2017, **125**, 143–189.

36 T. Liang, X. Sun, W. Li, G. Hou and F. Gao, 1,2,3-Triazole-Containing Compounds as Anti–Lung Cancer Agents: Current Developments, Mechanisms of Action, and Structure–Activity Relationship, *Front. Pharmacol*, 2021, **12**, 661173.

37 K. I. Slavova, L. T. Todorov, N. P. Belskaya, M. A. Palafox and I. P. Kostova, Developments in the Application of 1,2,3-Triazoles in Cancer Treatment, *Recent Pat. Anti-Cancer Drug Discovery*, 2020, **15**(2), 92–112.

38 D. Veeranna, L. Ramdas, G. Ravi, S. Bujji, V. Thumma and J. Ramchander, Synthesis of 1,2,3-Triazole Tethered Indole Derivatives: Evaluation of Anticancer Activity and Molecular Docking Studies, *ChemistrySelect*, 2022, **7**(29), e202201758.

39 J. A. Mokariya, R. C. Patel, D. P. Rajani and M. P. Patel, Synthesis of novel indole-oxindole clubbed 1, 2, 3-triazole hybrids: antimicrobial evaluation and molecular docking study, *Res. Chem. Intermed.*, 2023, **49**(7), 2933–2953.

40 S. Shafi, M. M. Alam, N. Mulakayala, C. Mulakayala, G. Vanaja, A. M. Kalle, R. Pallu and M. S. Alam, Synthesis of novel 2-mercapto benzothiazole and 1,2,3-triazole based bis-heterocycles: their anti-inflammatory and anti-nociceptive activities, *Eur. J. Med. Chem.*, 2012, **49**, 324–333.

41 R. S. Keri, S. A. Patil, S. Budagumpi and B. M. Nagaraja, Triazole: A Promising Antitubercular Agent, *Chem. Biol. Drug Des.*, 2015, **86**(4), 410–423.

42 Y. Tian, Z. Liu, J. Liu, B. Huang, D. Kang, H. Zhang, E. De Clercq, D. Daelemans, C. Pannecouque, K. H. Lee, C. H. Chen, P. Zhan and X. Liu, Targeting the entrance channel of NNIBP: Discovery of diarylnicotinamide 1,4-disubstituted 1,2,3-triazoles as novel HIV-1 NNRTIs with high potency against wild-type and E138K mutant virus, *Eur. J. Med. Chem.*, 2018, **151**, 339–350.

43 R. Kumar, L. Vats, S. Bua, C. T. Supuran and P. K. Sharma, Design and synthesis of novel benzenesulfonamide containing 1,2,3-triazoles as potent human carbonic anhydrase isoforms I, II, IV and IX inhibitors, *Eur. J. Med. Chem.*, 2018, **155**, 545–551.

44 D. Baraniak and J. Boryski, Triazole-Modified Nucleic Acids for the Application in Bioorganic and Medicinal Chemistry, *Biomedicines*, 2021, **9**(6), 628.

45 A. Ben Ali, Y. El Bakri, C. H. Lai, J. Sebhaoui, L. El Ghayati, E. M. Essassi and J. T. Mague, Crystal structure, computational study and Hirshfeld surface analysis of ethyl (2S,3R)-3-(3-amino-1H-1,2,4-triazol-1-yl)-2-hy-droxy-3-phenyl-propano-ate, *Acta Crystallogr., Sect. E: Crystallogr. Commun.*, 2019, **75**(Pt 12), 1919–1924.

46 B. F. Abdel-Wahab, B. M. Kariuki, H. A. Mohamed, M. S. Bekheit, H. M. Awad and G. A. El-Hiti, Synthesis and anticancer activity of 3-(1-aryl-5-methyl-1H-1, 2, 3-triazol-4-yl)-1-phenyl-1H-pyrazole-4-carbaldehydes, *J. Mol. Struct.*, 2023, **1294**, 136528.

47 K. Sanphanya, S. K. Wattanapitayakul, S. Phowichit, V. V. Fokin and O. Vajragupta, Novel VEGFR-2 kinase inhibitors identified by the back-to-front approach, *Bioorg. Med. Chem. Lett.*, 2013, **23**(10), 2962–2967.

48 B. Banerji, K. Chandrasekhar, K. Sreenath, S. Roy, S. Nag and K. D. Saha, Synthesis of Triazole-Substituted Quinazoline Hybrids for Anticancer Activity and a Lead Compound as the EGFR Blocker and ROS Inducer Agent, *ACS Omega*, 2018, **3**(11), 16134–16142.

49 L. Bekaert, S. Valable, E. Lechapt-Zalcman, K. Ponte, S. Collet, J. M. Constans, G. Levallet, K. Bordji, E. Petit, P. Branger, E. Emery, A. Manrique, L. Barré, M. Bernaudin and J. S. Guillamo, [18F]-FMISO PET study of hypoxia in gliomas before surgery: correlation with molecular markers of hypoxia and angiogenesis, *Eur. J. Nucl. Med. Mol. Imaging*, 2017, **44**(8), 1383–1392.

50 L. G. Nicely, R. M. Vala, D. B. Upadhyay, J. Nogales, C. Chi, S. Banerjee and H. M. Patel, One-pot two-step catalytic synthesis of 6-amino-2-pyridone-3,5-dicarbonitriles enabling anti-cancer bioactivity, *RSC Adv.*, 2022, **12**(37), 23889–23897.

51 V. Tandon, R. M. Vala, A. Chen, R. L. Sah, H. M. Patel, M. C. Pirrung and S. Banerjee, Syrbactin-class dual constitutive- and immuno-proteasome inhibitor TIR-199 impedes myeloma-mediated bone degeneration in vivo, *Biosci. Rep.*, 2022, **42**(2), BSR20212721.

52 S. Banerjee, T. Wei, J. Wang, J. J. Lee, H. L. Gutierrez, O. Chapman, S. E. Wiley, J. E. Mayfield, V. Tandon, E. F. Juarez, L. Chavez, R. Liang, R. L. Sah, C. Costello, J. P. Mesirov, L. de la Vega, K. L. Cooper, J. E. Dixon, J. Xiao and X. Lei, Inhibition of dual-specificity tyrosine phosphorylation-regulated kinase 2 perturbs 26S proteasome-addicted neoplastic progression, *Proc. Natl. Acad. Sci. U. S. A.*, 2019, **116**(49), 24881–24891.

53 A. Keenlyside, T. Marples, Z. Gao, H. Hu, L. G. Nicely, J. Nogales, H. Li, L. Landgraf, A. Solth, A. Melzer, K. Hossain-Ibrahim, Z. Huang, S. Banerjee and J. Joseph, Development and optimisation of in vitro sonodynamic therapy for glioblastoma, *Sci. Rep.*, 2023, **13**(1), 20215.

54 S. Banerjee, A. Zagorska, M. Deak, D. G. Campbell, A. R. Prescott and D. R. Alessi, Interplay between Polo kinase, LKB1-activated NUAK1 kinase, PP1 beta(MYPT1) phosphatase complex and the SCF beta TrCP E3 ubiquitin ligase, *Biochem. J.*, 2014, **461**, 233–245.

55 J. Bain, L. Plater, M. Elliott, N. Shpiro, C. J. Hastie, H. McLauchlan, I. Klevernic, J. S. Arthur, D. R. Alessi and P. Cohen, The selectivity of protein kinase inhibitors: a further update, *Biochem. J.*, 2007, **408**(3), 297–315.

56 S. Banerjee, S. J. Buhrlage, H.-T. Huang, X. Deng, W. Zhou, J. Wang, R. Traynor, A. R. Prescott, D. R. Alessi and N. S. Gray, Characterization of WZ4003 and HTH-01-015 as selective inhibitors of the LKB1-tumour-suppressor-activated NUAK kinases, *Biochem. J.*, 2014, **457**, 215–225.

57 A. Daina, O. Michielin and V. Zoete, SwissADME: a free web tool to evaluate pharmacokinetics, drug-likeness and medicinal chemistry friendliness of small molecules, *Sci. Rep.*, 2017, **7**(1), 42717.